C. R. Acad. Sci. Paris, t. 2, Série IV, p. 1073–1089, 2001
Physique appliquée/*Applied physics*
(Biophysique/*Biophysics*)



## IMAGERIE ACOUSTIQUE ET OPTIQUE DES MILIEUX BIOLOGIQUES

## *OPTICAL AND ACOUSTICAL IMAGING OF BIOLOGICAL MEDIA*

# Diffuse optical imaging and spectroscopy, in vivo

**Amir H. GANDJBAKHCHE**

**Laboratory of Integrative and Medical Biophysics, National Institute of Child Health and Human Development, National Institutes of Health, Bethesda, MD 20892, USA**
**E-mail: amir@helix.nih.gov**

**(Reçu le 10 juillet 2001, accepté le 11 juillet 2001)**

**Abstract.** Based on photon migration the new goal of diffuse optical imaging is to reveal optical contrasts in the depth of biological tissues. We discuss first the origin of contrast mechanism (absorption, fluorescence and scattering) used on diffuse optical imaging and spectroscopy. Then, various experimental approaches are described based on CW, pulsed and modulated light excitation and detection. Theoretical models which provide solutions for direct and inverse problems are presented using random walk theory. Finally two studies on breast imaging and on the use of fluorescence exogeneous markers are discussed in detail. Publié par Éditions scientifiques et médicales Elsevier SAS

**scattering / fluorescence / absorption / tomography / optical biopsy / biological tissues**

### *Imagerie et spectroscopie in-vivo en lumière diffuse*

**Résumé.** *Le but de l'imagerie en lumière diffuse, basée sur la marche aléatoire des photons, est de révéler des contrastes optiques dans la profondeur des tissus biologiques. Nous discutons d'abord de l'origine du contraste (lié à l'absorption, à la fluorescence ou à la diffusion) utilisé en imagerie et en spectroscopie en lumière diffuse. Puis, diverses approches expérimentales, basées sur une excitation et une détection en régime continue, impulsionnelle ou modulée sont décrites. Les modèles théoriques qui permettent d'atteindre les solutions des problèmes directs ou inverses sont présentés dans le contexte de la théorie de la marche aléatoire. Enfin, deux études sur l'imagerie du sein et sur l'utilisation de marqueurs exogènes fluorescents sont discutés en détail. Publié par Éditions scientifiques et médicales Elsevier SAS*

***diffusion / fluorescence / absorption / tomographie / biopsie optique / tissus biologiques***

## 1. Introduction

In the last two decades, developments in lasers, high speed scanners, and modern electro-optical imaging devices have led to sophisticated technologies such as fluorescence microscopy and confocal microscopy, which have contributed to great discoveries in molecular and cell biology. These achievements were predominantly based on studies of single cells or in-vitro tissue cultures. Virtually all the current optical imaging systems are based on geometric optics of light rays passing through the objects of interest. Most tissues scatter light so strongly, however, that for geometric optics-based equipment to work, special techniques are needed to remove multiply scattered light (such as pinholes in confocal imaging or

**Note présentée par Guy LAVAL.**

S1296-2147(01)01251-3/FLA
Publié par Éditions scientifiques et médicales Elsevier SAS.

interferometry in optical coherence microscopies). Even with these special designs, high-resolution optical imaging fails at depths of more than 500 microns below the tissue surface. As a result, in-vivo optical imaging traditionally has been limited to superficial tissue surfaces directly or endoscopically accessible, and to tissues with a biological window (e.g., along the optical axis of the eye).

Because collimated visible or infrared (IR) light impinging upon thick tissue is scattered many times in a distance of $\sim 1$ mm, the analysis of light-tissue interactions requires theories based on the diffusive nature of light propagation. In contrast to X-ray and Positron Emission Tomography (PET), a complex underlying theoretical picture is needed to describe photon paths as a function of scattering and absorption properties of the tissue.

Approximately a decade ago, a new field called 'photon migration' was born that seeks to characterize the statistical physics of photon motion through turbid tissues. The research goal has been 3D imaging of macroscopic structures at greater depths within tissues and to provide reliable pathlength estimation for noninvasive spectral analysis of tissue changes. Although geometrical optics fails to describe light propagation under these conditions, the statistical physics of strong, multiply scattered light provides powerful approaches to macroscopic imaging and subsurface detection and characterization. Therefore, one of the 'biomedical optics' tasks is to design new approaches for non-invasive quantitative optical spectroscopic and tomographic imaging of tissue structures for clinical assessment of physiological parameters and metabolic status. These techniques offer a variety of functional imaging modalities, in addition to density imaging, while avoiding ionizing radiation hazards.

In Section 2, contrast mechanisms used in diffuse optical imaging and spectroscopy are presented. Section 3 is devoted to differing methods of measurements. Theoretical models for spectroscopy and imaging are discussed in Section 4. In Sections 5 and 6, two studies that we are pursuing on breast imaging and use of exogenous fluorescent markers will be presented in detail. Finally, we conclude in Section 7.

## 2. Contrast mechanisms in tissue optics

The major challenge of tissue optics is to define optical parameters related to the physiological properties of tissue, which can be used to differentiate structures and functional status in-vivo. Definition of these parameters is dictated by the way light interacts with a turbid media such as tissue. Naturally two approaches can be taken. The first is based on the wave interpretation of light which leads to the use of Maxwell's equations, and therefore to quantify the spatially varying permittivity as a measurable quantity. For simplicity and historic reasons, the particle interpretation of light has been mostly used (see Section 4). In photon transport theory, one considers the behavior of discrete photons as they move through the tissue. This motion is characterized by absorption and scattering, and when interfaces (e.g., layers) are involved, refraction. The absorption coefficient, $\mu_a$ ($mm^{-1}$) represents the inverse mean pathlength of photon before absorption. $1/\mu_a$ is also the distance in a medium where intensity is attenuated by a factor of $1/e$ (Beer's Lambert Law). Absorption in tissue is strongly wavelength dependent and is due to chromophores and water. Among the chromophores in tissue, the dominant component is the hemoglobin in blood. In *figure 1*, hemoglobin absorption by type is presented. As seen in this figure, in the visible range the blood absorption is relatively high compared to absorption in the near infrared. By contrast, water absorption is low in the visible and NIR region and increases rapidly above approximately 950 nm. Thus, for greatest penetration of light in tissue, wavelengths in the 650–950 nm spectrum are mostly used. This region of the light spectrum is called 'the therapeutic window.' One should note that different spectra of chromophores allow one to separate the contribution of varying functional species in tissue (e.g., quantification of oxy-and deoxy-hemoglobin to study tissue oxygenation).

Similarly, scattering is characterized by a coefficient, $\mu_s$, that is the inverse mean free path of photons between scattering events. Average size of the scatterers in tissue, in proportion to the wavelength of the light, places the scattering in the Mie region. In the Mie region, a scattering event does not result in isotropic scattering angles [1,2]. Instead, the scattering in tissue is biased in the forward direction.

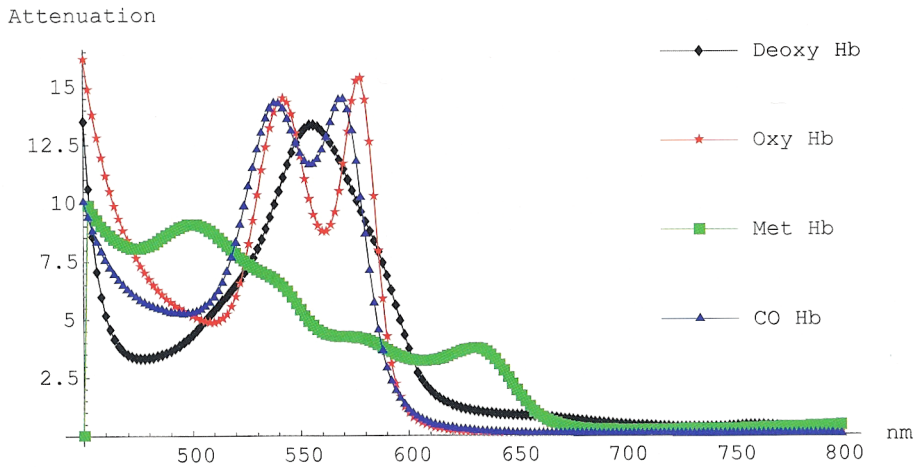


**Figure 1.** Attenuation of photons in hemoglobin as a function of wavelength.

For example, by studying the development of neonatal skin, Saidi et al. [3] were able to show that the principal sources of anisotropic scattering in muscle are collagen fibers. The fibers were determined to have a mean diameter of 2.2 microns. In addition to the Mie scattering from the fibers, there is isotropic Rayleigh scattering due to the presence of much smaller scatterers such as organelles in cells.

Anisotropic scattering is quantified in a coefficient, $g$, which is defined as the mean cosine of the scattering angle. Where $p(\theta)$ is the probability of a particular scattering angle,

$$g \equiv \langle \cos(\theta) \rangle \equiv \frac{\int_0^\pi p(\theta) \cos(\theta) \sin(\theta)\, \mathrm{d}\theta}{\int_0^\pi p(\theta) \sin(\theta)\, \mathrm{d}\theta} \tag{1}$$

For isotropic scattering, $g = 0$. For complete forward scattering, $g = 1$, and for complete back scattering, $g = -1$. In tissue, $g$ is typically 0.7 to 0.98 [3–5].

Likewise, different tissue types have differing scattering properties, which are also wavelength dependent. The scattering coefficients of many soft tissues have been measured at a variety of optical wavelengths, and are within the range 10–100 $\mathrm{mm}^{-1}$. In comparison to absorption, however, scattering changes, as a function of wavelength, are more gradual and have smaller extremes. Abnormal tissues such as tumors, fibro-adenomas and cysts all have scattering properties that are different from normal tissue [6,7]. Thus, the scattering coefficient of an inclusion may also be an important clue to diagnostic.

Theories of photon migration are often based on isotropic scattering. Therefore, one must find the appropriate scaling relationships that will allow one to use an isotropic scattering model. For the case of diffusion like models (e.g., [8]), it has been shown that one may use an isotropic scattering model with a corrected scattering coefficient, $\mu_\mathrm{s}'$, and obtain equivalent results where:

$$\mu_\mathrm{s}' = \mu_\mathrm{s}(1 - g) \tag{2}$$

The corrected scattering coefficient is smaller than the actual scattering which corresponds to a greater distance between isotropic scattering events than would occur with anisotropic scattering. For this reason, $\mu_\mathrm{s}'$ is typically called the transport-corrected scattering coefficient.

There are instances in which the spectroscopic signatures will not be sufficient for detection of disease. This can occur when the specific disease results in only very small changes to the tissue scattering and absorption properties, or when the scattering and absorption properties of the disease are not unique to

the disease. Although it is not clear what the limits of detectability are in relationship to diseased tissue properties, it is clear that there will be cases for which optical techniques based on elastic absorption are inadequate. In such cases, another source of optical contrast, such as fluorescence, will be required to detect and locate the disease. Presence of fluorescent molecules in tissues can provide useful contrast mechanisms. Concentration of these endogenous fluorophores in the body can be related to functional and metabolic activities, and therefore to the disease processes. For example, concentration of fluorescent molecules such as collagen, NADH have been used to differentiate between normal and abnormal tissue (see excellent review in [9]).

Advances in molecular biology of diseased processes, new immunohistopathological techniques, and the development of fluorescently-labeled cell surface markers have led to a revolution in specific molecular diagnosis of disease by histopathology, as well as in research on molecular origins of disease processes (e.g., using fluorescence microscopy in cell biology). As a result, an exceptional level of specificity is now possible due to the advances in the design of exogenous markers. Molecules can now be tailor-made to bind only to specific receptor sites in the body. These receptor sites may be antibodies or other biologically interesting molecules. Fluorophores may be bound to these engineered molecules and injected into the body, where they will preferentially concentrate at specific sites of interest [10,11].

Furthermore, fluorescence may be used as a probe to measure environmental conditions in a particular locality by capitalizing on changes in fluorophore lifetimes [12,13]. Each fluorophore has a characteristic lifetime that quantifies the probability of a specific time delay between fluorophore excitation and emission. In practice, this lifetime may be modified by specific environmental factors such as temperature, pH, and concentrations of substances such as $O_2$. In these cases, it is possible to quantify local concentrations of specific substances or specific environmental conditions by measuring the lifetime of fluorophores at the site. Whereas conventional fluorescence imaging is very sensitive to non-uniform fluorophore transport and distribution (for example, blood does not transport molecules equally to all parts of the body), fluorescence lifetime imaging is insensitive to transport non-uniformity as long as a detectable quantity of fluorophores is present in the site of interest. Throughout the following Sections, experimental techniques and differing models used to quantify these sources of optical contrast will be presented.

## 3. Measurable quantities and experimental techniques

Three classes of measurable quantities prove to be of interest in transforming results of remote sensing measurements in tissue into useful physical information. The first is the spatial distribution of light or the intensity profile generated by photons re-emitted through a surface and measured as a function of the radial distance from the source and the detector when the medium is continually irradiated by a point source (often a laser). This type of measurement is called Continuous Wave (CW). The intensity, nominally, does not vary in time. The second class is the temporal response to a very short pulse ($\sim$ picosecond) of photons impinging on the surface of the tissue. This technique is called time-resolved and the temporal response is known as the time-of-flight (TOF). The third class is the frequency-domain technique in which an intensity-modulated laser beam illuminates the tissue. In this case the measured outputs are the AC modulation amplitude and the phase shift of the detected signal. These techniques could be implemented in geometries with different arrangements of source(s) and detector(s):

(a) in the reflection mode, source(s) and detector(s) are placed at the same side of the tissue;
(b) in the transmission mode, source(s) and detector(s) are located on opposite sides of the tissue. In the latter, source and detector can move in tandem while scanning the tissue surface. Detectors with lateral offsets also can be used;
(c) tomographic sampling often uses multiple sources and detectors placed around the circumference of the target tissue.

For CW measurements the instrumentation is simple and requires only a set of light sources and detectors. In this technique the only measurable quantity is the intensity of light, and, due to multiple scattering, strong

pathlength dispersion occurs which results in a loss of localization and resolution. Hence, this technique is widely used for spectroscopic measurements of bulk tissue properties in which the tissue is considered to be homogeneous [14,15]. However, CW techniques for imaging abnormal targets, which use only the coherent portion of light, and thereby reject photons with long paths, have also been investigated. Using the transillumination geometry, collimated detection is used to isolate un-scattered photons [16–18]. Spatial filtering has been proposed which employs a lens to produce the Fourier spectrum of the spatial distribution of light from which the high-order frequencies are removed. The resulting image is formed using only the photons with angles close to normal [19]. Polarization discrimination has been used to select those photons which undergo few scattering events and therefore preserve a fraction of their initial polarization state, as opposed to those photons which experience multiple scattering resulting in complete randomization of their initial polarization state [20]. Several investigators have used heterodyne detection which involves measuring the beat frequency generated by the spatial and temporal combination of a light beam and a frequency modulated reference beam. Constructive interference occurs only for the coherent portion of the light [21–23]. However, the potential of direct imaging using CW techniques in very thick tissue (e.g., breast) has not been established. On the other hand, use of models of photon migration implemented in inverse method based on backprojection techniques has shown promising results. For example, Phillips Medical has used 256 optical fibers placed at the periphery of a white conical shaped vessel. The target under interrogation, in this case the breast, is suspended in the vessel, and surrounded by a matching fluid. Three CW laser diodes sequentially illuminate the breast using one fiber. The detection is done simultaneously by 255 fibers. It is now clear that CW imaging cannot provide direct images with clinically acceptable resolution in thick tissue. Attempts are underway to devise inverse algorithms to separate the effects of scattering and absorption and therefore use this technique for quantitative spectroscopy as proposed by Phillips [24]. However, until now, clinical application of CW technique in imaging has been limited by the mixture of scattering and absorption of light in the detected signal. To overcome this problem, time-dependent measurement techniques have been investigated.

Time-domain techniques involve the temporal resolution of photons traveling inside the tissue. The basic idea is that photons with smaller pathlengths are those that arrive earlier to the detector. In order to discriminate between un-scattered or less scattered light and the majority of the photons, which experience a large number of multiple scattering, sub-nanosecond resolution is needed. This short time gating of an imaging system requires the use of a variety of techniques involving ultra-fast phenomena and/or fast detection systems. Ultra-fast shuttering is performed using Kerr effect. The birefringence in the Kerr cell, placed between two crossed polarizers, is induced using very short pulses. Transmitted light through the Kerr cell is recorded, and temporal resolution of a few picoseconds is achieved [25]. When an impulse of light ($\sim$ picoseconds or hundreds of femtoseconds) is launched at the tissue surface, the whole temporal distribution of photon intensity can be recorded by a streak camera. The streak camera can achieve temporal resolution on the order of few picoseconds up to several nanosececonds detection time. This detection system has been widely used to assess the performance of breast imaging and neonatal brain activity [26,27]. The time of flight recorded by the streak camera is the convolution of the pulsed laser source (in practice with a finite width) and the actual Temporal Point Spread Function (TPSF) of the diffuse photons. Instead of using very short pulse lasers (e.g., Ti–saphire lasers), the advent of pulse diode lasers with relatively larger pulse width (100–400 psec) have brought the cost of time-domain imaging much lower. However, deconvolution of the incoming pulse and the detected TPSF has been a greater issue. Along with diode laser sources, several groups have also used time-correlated single photon counting with photomultipliers for recording the TPSF [28,29]. Fast time gating is also obtained by using Stimulated Raman Scattering. This phenomenon is a non-linear Raman interaction in some materials such as hydrogen gas involving the amplification of photons with Stokes shift by a higher energy pump beam. The system operates by amplifying only the earliest arriving photons [30]. Less widely used techniques such as second-harmonic generation [31], parametric amplification [32] and a variety of others have been proposed for time-domain (see an excellent review in [33]).

For frequency-domain measurements, the requirement is to measure the DC amplitude, the AC amplitude, and the phase shift of the photon density wave. For this purpose a CW light source is modulated with a given frequency ($\sim$ 100 MHz). Lock-in Amplifiers and/or phase sensitive CCD camera have been used to record the amplitude and phase [34,35]. Multiple sources at different wavelengths can be modulated with a single frequency or multiple frequencies [36,37]. In the latter case network analyzer is used to produce modulation swept from several hundreds of MHz to up to 1 GHz.

## 4. Models of photon migration in tissue

Photon migration theories in biomedical optics have been borrowed from other fields such as astrophysics, atmospheric science, and specifically from nuclear reactor engineering [38,39]. The common properties of these physical media and biological tissues are their characterization by element of randomness in both space and time. Because of many difficulties surrounding development of a theory based on a detailed picture of the microscopic processes involved in the interaction of light and matter, investigations are often based on statistical theories These can take a variety of forms, ranging from quite detailed multiple-scattering theories [39] to transport theory [40]. However, the most widely used theory is the time-dependent diffusion approximation to the transport equation:

$$\vec{\nabla} \cdot \left(D\vec{\nabla}\Phi(\vec{r},t)\right) - \mu_{\mathrm{a}}\Phi(\vec{r},t) = \frac{1}{c}\frac{\partial\Phi(\vec{r},t)}{\partial t} - S(\vec{r},t) \tag{3}$$

Where $\vec{r}$ and $t$ are spatial and temporal variables, $c$ is the speed of light in tissue, and $D$ is the diffusion coefficient related to the absorption and scattering coefficients as follows:

$$D = \frac{1}{3[\mu_{\mathrm{a}} + \mu'_{\mathrm{s}}]} \tag{4}$$

The quantity $\Phi(\vec{r},t)$ is called the fluence, defined as the power incident on an infinitesimal volume element divided by its area. Note that the equation does not incorporate any angular dependence, therefore assumes an isotropic scattering. However, for the use of the diffusion theory for anisotropic scattering, the diffusion coefficient is expressed in terms of transport-corrected scattering coefficient. $S(\vec{r},t)$ is the source term. The gradient of fluence, $J(\vec{r},t)$, at the tissue surface is the measured flux of photons by the detector:

$$J(\vec{r},t) = -D\vec{\nabla}\Phi(\vec{r},t) \tag{5}$$

For CW measurement, the time-dependence of the flux vanishes, and the source term can be seen as the power impinging in its area. For time resolved measurement, the source term is a Dirac delta function describing a very short impulse of photon. Equation (3) has been solved analytically for different types of measurements such as reflection and transmission mode assuming that the optical properties remain invariant through the tissue. To incorporate the finite boundaries, the method of images has been used. In the simplest case, the boundary has been assumed to be perfectly absorbing which does not take into account the difference between indices of refraction at the tissue–air interface. For semi-infinite and transillumination geometries a set of theoretical expressions has been obtained for time-resolved measurements [41].

The diffusion approximation equation in the frequency-domain is the Fourier transform of the time-domain in respect to time. Fourier transform applied to the time–dependent diffusion equation leads to a new equation:

$$\vec{\nabla} \cdot \left(D\vec{\nabla}\Phi(\vec{r},\omega)\right) - \left[\mu_{\mathrm{a}} + \frac{\mathrm{i}\omega}{c}\right]\Phi(\vec{r},\omega) + S(\vec{r},\omega) = 0 \tag{6}$$

Here the time variable is replaced by the frequency $\omega$. This frequency is the modulation angular frequency of the source. In this model, the fluence can be seen as a complex number describing the amplitude and

phase of the photon density wave, dumped with a DC component:

$$\Phi(\vec{r},\omega) = \Phi_{\mathrm{AC}}(\vec{r},\omega) + \Phi_{\mathrm{DC}}(\vec{r},0) = I_{\mathrm{AC}}\exp(\mathrm{i}\theta) + \Phi_{\mathrm{DC}}(\vec{r},0) \tag{7}$$

In the r.h.s. of equation (6), the quantity $\theta$ is the phase shift of the diffusing wave. For a non-absorbing medium, its wavelength is:

$$\lambda = 2\pi\sqrt{\frac{2c}{3\mu_{\mathrm{s}}'\omega}} \tag{8}$$

Likewise in the time-domain, equation (6) has an analytical solution for the case that the tissue is considered homogeneous. The analytical solution permits one to deduce the optical properties in a spectroscopic setting.

For imaging where the goal is to distinguish between structures in tissue, the diffusion coefficient and the absorption coefficient in equations (3) and (6) become spatial-dependent and be replaced by $D(r)$ and $\mu_{\mathrm{a}}(r)$. For the cases that an abnormal region is embedded in otherwise homogeneous tissue, perturbation methods based on Born approximation or Rytov approximation have been used (see excellent review in [42]). However for the cases that the goal is to reconstruct the spectroscopic signatures inside the tissue, no analytical solution exists. For these cases inverse algorithms are devised to map the spatially varying optical properties. Numerical methods such as finite-element or finite difference methods have been used to reconstruct images of breast, brain, and muscle [43–45]. Furthermore, in those cases that structural heterogeneity exists, a priori information can be used by differing image modalities such as MRI. An example is given in *figure 2, a–d*. Combining MRI and NIR imaging, rat cranium functional imaging during changes in inhaled oxygen concentration has been studied [46]. *Figures 2a* and *2b* correspond to the MRI image and the corresponding constructed finite element mesh. *Figures 2c* and *2d* correspond to the oxygen map of the brain with and without incorporation of MRI geometry and constraints.

Clearly the use of MRI images have improved dramatically the resolution of the oxygen map. The use of optical functional imaging in conjunction with other imaging modalities have open new possibilities in the image and treat of diseases at the bedside.

The second theoretical framework used in tissue optics is the Random Walk Theory (RWT) on a lattice developed at the National Institutes of Health [46] and historically precedes the use of the diffusion approximation theory. It has been shown that RWT may be used to derive an analytical solution for the distribution of photon path-lengths in turbid media such as tissue [47]. RWT models the diffusion-like motion of photons in turbid media in a probabilistic manner. Using RWT, an expression may be derived for the probability of a photon arriving at any point and time given a specific starting point and time.

Tissue may be modeled as a 3D cubic lattice containing a finite inclusion, or region of interest, as shown in *figure 3*. The medium has an absorbing boundary corresponding to the tissue surface, and the lattice spacing is proportional to the mean photon scattering distance, $1/\mu_{\mathrm{s}}$. The behavior of photons in the RWT model is described by three dimensionless parameters, $\rho$, $n$, $\mu$, which are respectively the radial distance, the number of steps, and the probability of absorption per lattice step. In the RWT model, photons may move to one of the six nearest neighboring lattice points, each with probability $1/6$. If we know the number of steps, $n$, taken by a photon traveling between two points on the lattice, then we also know the length of the photon path.

RWT is useful in predicting the probability distribution of photon path-lengths over distances of at least 5 mean-photon scattering distances. The derivation of these probability distributions is described in a review paper [48]. For simplicity in this derivation, the tissue–air interface is considered to be perfectly absorbing; a photon arriving at this interface is counted as arriving at a detector on the tissue surface. The derivation uses the Central Limit Theorem and a Gaussian distribution around lattice points to obtain a closed-form solution that is independent of the lattice structure.

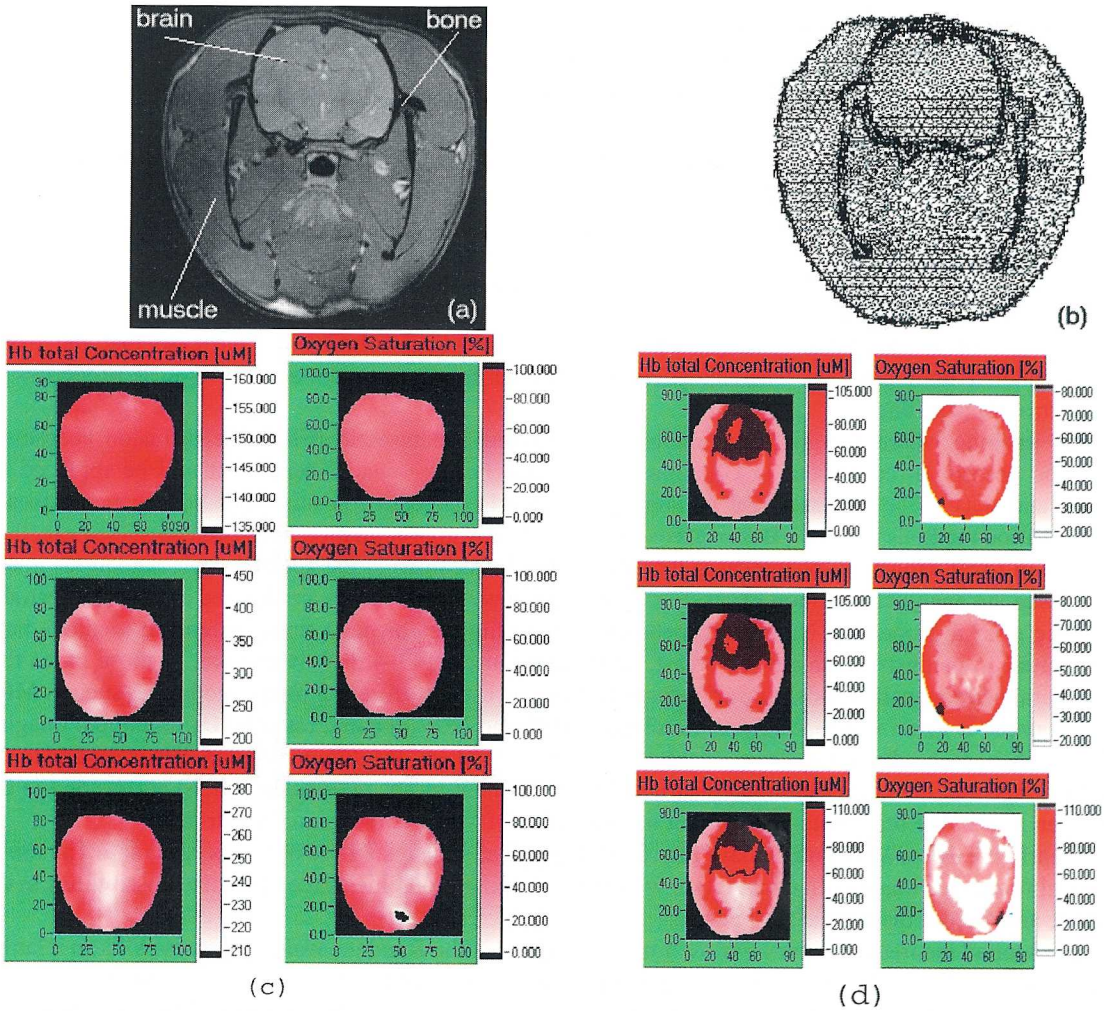


**Figure 2.** Functional imaging of rat cranium during changes in inhaled oxygen concentration. (a) MRI image; (b) creation of the mesh to distinguish different compartments in the brain; (c) Map of hemoglobin concentration and oxygen saturation of the rat brain without structural constraints from MRI; (d) Same as (c) with structural constraints including tissue heterogeneity. In (c) and (d) the rows from top correspond to 13%, 8%, 0% (after death) oxygen inhaled (Courtesy of Dartmouth College).

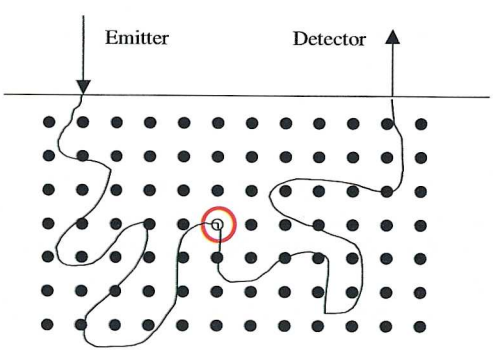


**Figure 3.** 2D Random Walk Lattice showing representative photon paths from an emitter to specific site and then to a detector.

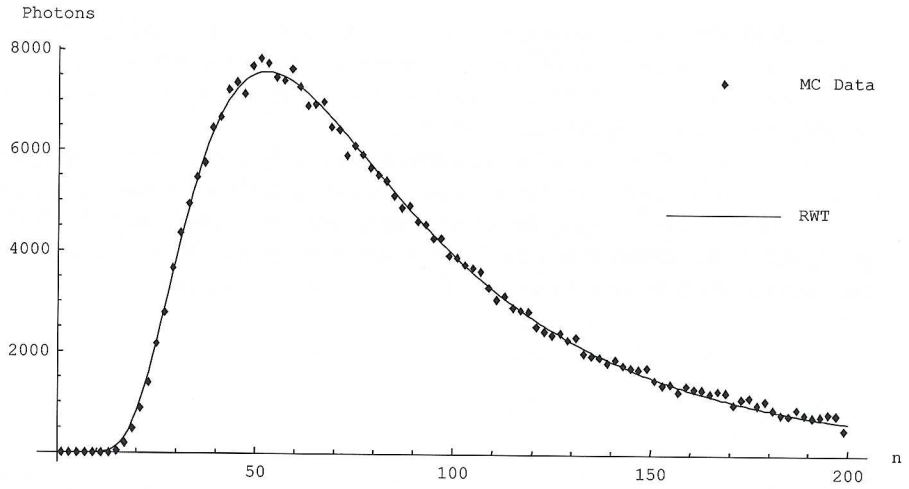


**Figure 4.** RWT prediction and Monte Carlo Simulation results for transillumination of a 15 mm thick slab with scattering $1/\text{mm}$ and $10^9$ photons.

The dimensionless RWT parameters, $\rho$, $n$, $\mu$, described above, may be transformed to actual parameters, in part, by using time, $t$, the speed of light in tissue, $c$, and distance traveled, $r$, as follows:

$$\rho \rightarrow \frac{r\mu_{\mathrm{s}}'}{\sqrt{2}}, \qquad n \rightarrow \mu_{\mathrm{s}}' ct, \qquad \mu \rightarrow \frac{\mu_{\mathrm{a}}}{\mu_{\mathrm{s}}'} \tag{9}$$

As was stated before, scattering in tissue is highly anisotropic. Therefore, one must find the appropriate scaling relationships that will allow one to use an isotropic scattering model such as RWT. Like diffusion theory, for RWT [49], it has been shown that one may use an isotropic scattering model with a corrected scattering coefficient, $\mu_{\mathrm{s}}'$, and obtain equivalent results. The corrected scattering coefficient is smaller than the actual scattering which corresponds to a greater distance between isotropic scattering events than would occur with anisotropic scattering. RWT has been used to show how one would transit from the use of $\mu_{\mathrm{s}}$ to $\mu_{\mathrm{s}}'$ as the distance under consideration increases [50].

As an example, for a homogeneous slab into which a photon has been inserted, the probability of a photon arriving at a point $\rho$ after $n$ steps is [51]:

$$P(n,\rho) = \frac{\sqrt{3}}{2}\left[\frac{1}{2\pi(n-2)}\right]^{3/2} \mathrm{e}^{-\frac{3}{2}\rho^2/(n-2)} \sum_{k=-\infty}^{\infty} \left[\mathrm{e}^{-\frac{3}{2}[(2k+1)L-2]^2/(n-2)} - \mathrm{e}^{-\frac{3}{2}[(2k+1)L]^2/(n-2)}\right] \mathrm{e}^{-n\mu} \tag{10}$$

where $L$ is the thickness of the slab. The method of images has been used to take into account the two boundaries of the slab. Plotting equation (10) yields a photon arrival curve as shown in *figure 4*; Monte Carlo simulation data are overlaid. In the next two sections the use of RWT for imaging will be presented.

## 5. RWT applied to quantitative spectroscopy of breast

One of the most challenging areas to apply diffuse optical imaging of deep tissues is the human breast (see review article in [52]). It is clear that any new imaging or spectroscopic modalities which can improve the diagnosis of breast tumors or can add new knowledge about the physiological properties of the breast and surrounding tissues will have a great significance in medicine.

Conventional transillumination using continuous wave (CW) light was used for breast screening several decades ago [53]. However, because of the high scattering properties of tissue, this method resulted in poor

resolution. In the late 1980s, time-resolved imaging techniques were proposed to enhance spatial resolution by detecting photons with very short time-of-flight within the tissue. In this technique a very short pulse (of $\sim$ picosecond duration) impinges upon the tissue. Photons experience dispersion in their pathlengths, resulting in temporal dispersion in their time-of-flight (TOF).

To evaluate the performance of time-resolved transillumination techniques, we used RWT on a lattice. Our analysis of breast transillumination was based on the calculation of the point spread function (PSF) of time resolved photons as they visit differing sites at different planes inside a finite slab. The PSF, $\{W_n\}$, is defined as the probability that a photon inserted into the tissue visits a given site, is detected at the $n$th step (i.e., a given time), and has the following rather complicated analytical expression:

$$W_n = \left[h(\alpha_-, \beta_-) - h(\alpha_-, \beta_+) - h(\alpha_+, \beta_-) + h(\alpha_+, \beta_+)\right] \tag{11}$$

$$h(\alpha, \beta) = \frac{\sqrt{\alpha} + \sqrt{\beta}}{n^{3/2}\sqrt{\pi\alpha\beta}}\, \mathrm{e}^{-(\sqrt{\alpha}+\sqrt{\beta})/n - n\mu_\mathrm{a}/\mu'_\mathrm{s}} \tag{12}$$

$$\alpha_\pm = \frac{3}{4}\left[x^2 + y^2 + \left(z \pm \frac{\sqrt{2}}{\mu'_\mathrm{s}}\right)^2\right]\mu'^2_\mathrm{s}, \qquad \beta_\pm = \frac{3}{4}\left[(x)^2 + (y)^2 + \left(z + \frac{\sqrt{2}}{\mu'_\mathrm{s}} \pm \frac{\sqrt{2}}{\mu'_\mathrm{s}}\right)^2\right]\mu'^2_\mathrm{s} \tag{13}$$

where $\{x, y, z\}$ are the coordinates of any location for which the PSF is calculated. Evaluation of time-resolved imaging showed that strong scattering properties of tissues prevent direct imaging of abnormalities [54]. Hence, devising theoretical constructs to separate the effects of the scattering from the absorption was proposed, thus allowing one to map the optical coefficients as spectroscopic signatures of an abnormal tissue embedded in thick, otherwise normal tissue. In this method, accurate quantification of the size and optical properties of the target becomes a critical requirement for the use of optical imaging at the bedside. Using RWT on a lattice to analyze the time-dependent contrast observed in time-resolved transillumination experiments and deduce the size and optical properties of the target and the surrounding tissue from these contrasts. For the theoretical construction of contrast functions, two quantities are needed. First, the set of functions $\{W_n\}$ defined before. Second, the set of functions $\{P_n\}$ defined as the probability that a photon is detected at the $n$th step (i.e., time) in a homogeneous medium (equation (10)).

To relate the contrast of the light intensity to the optical properties and location of abnormal targets in the tissue, one can take advantage of some features of the theoretical framework. One feature is that the early time response is most dependent on scattering perturbations, whereas the late time behavior is most dependent on absorptive perturbations, thus allowing one to separate the influence of scattering and absorption perturbations on the observed image contrast. Increased scattering in the abnormal target is modeled as a time delay. Moreover, it was shown that the scattering contrast is proportional to the time-derivative of the PSF, $\mathrm{d}W_n/\mathrm{d}n$, divided by $P_n$ [55]. The second interesting feature in RWT methodology assumes that the contrast from scattering inside the inclusion is proportional to the cross section of the target (in the $z$ direction), instead of depending on its volume as modeled in the perturbation analysis [56].

Several research groups intend to implement their theoretical expressions into general inverse algorithms for optical tomography, i.e., to reconstruct three-dimensional maps of spatial distributions of tissue optical characteristics [52], and thereby quantify optical characteristics, positions and sizes of abnormalities. Unlike these approaches, our method is a multi-step analysis of the collected data. From images observed at differing flight times, we construct the time-dependent contrast functions, fit our theoretical expressions, and compute the optical properties of the background, and those of the abnormality along with its size. The outline of our data analysis is given in [56].

By utilizing our method for different wavelengths, one can obtain diagnostic information (for example, estimates of blood oxygenation of the tumor) for corresponding absorption coefficients that no other imaging modality can provide directly. Several research groups have already successfully used multi-wavelength measurements using frequency-domain techniques, to calculate physiological parameters (oxygenation, lipid, water) of breast tumors (diagnosed with other modalities) and normal tissue [57].

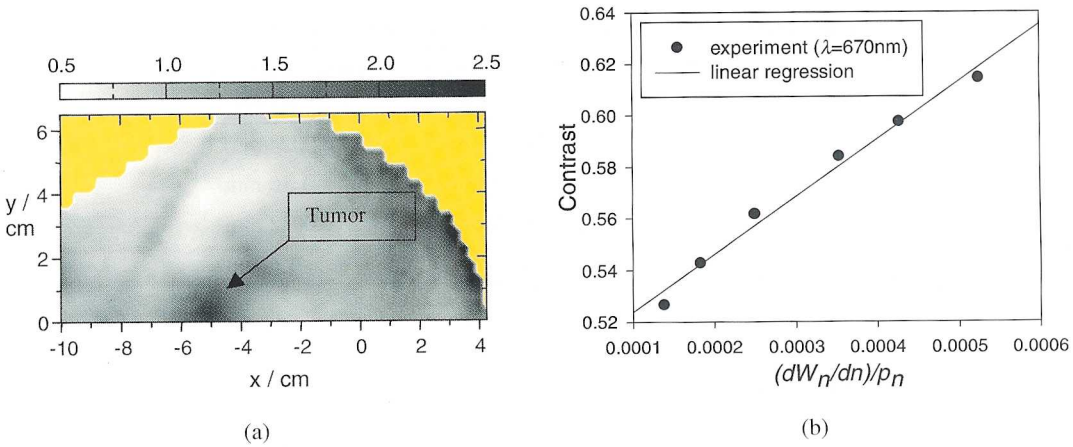


**Figure 5.** (a) 2D optical image of the breast with the tumor (Courtesy of Physikalich.-Techniche-Bundesanstalt, Berlin). (b) Contrast obtained from linear scan through the tumor plotted versus the derivative of PSF. From the linear regression the scattering coefficient of the tumor is deduced.

Researchers at Physikalich.-Techniche-Bundesanstalt (PTB) of Berlin have designed a clinically practical optical imaging system, capable of implementing time-resolved in-vivo measurements on human breast [29]. The breast is slightly compressed between two plates. A scan of the whole breast takes but a few minutes and can be done in mediolateral and craniocaudal geometries. The first goal is to quantify the optical parameters at several wavelengths and thereby estimate blood oxygen saturation of the tumor and surrounding tissue under the usual assumption that the chromophores contributing to absorption are oxy- and deoxy-hemoglobin and water. As an example, two sets of data, obtained at two wavelengths (670 and 785 nm), for a patient (84 year old) with invasive ductal carcinoma, were analyzed. Though the images exhibit poor resolution, the tumor can be easily seen in the optical image shown in *figure 5a*. In this figure, the image is obtained from reciprocal values of the total integrals of the distributions of times of flight of photons, normalized to a selected 'bulk' area. The tumor center is located at $x = -5$, $y = 0.25$ mm.

The best spatial resolution is observed, as expected, for shorter time-delays allowing one to determine the position of the tumor center on the 2D image (transverse coordinates) with accuracy $\sim 2.5$ mm. After preliminary data processing that includes filtering and deconvolution of the raw time-resolved data, we created linear contrast scans passing through the tumor center and analyzed these scans, using our algorithm. It is striking that one observes similar linear dependence of the contrast amplitude on the derivative of PSF (at 670 nm), as expected in our model (see *figure 5b*). The slope of this linear dependence was used, to estimate amplitude of the scattering perturbation [56].

Dimensions and values of optical characteristics of the tumor and surrounding tissues were then reconstructed for both wavelengths. Results show that the tumor had larger absorption and scattering than the background. Estimated parameters are presented in *table 1*.

Both absorption and scattering coefficients of the tumor and background all proved to be larger at the red wavelength (670 nm). Comparison of the absorption in the red and near infrared range is used to estimate blood oxygen saturation of the tumor and background tissue. Preliminary results of our analysis gave evidence that the tumor tissue is in a slightly deoxygenated state with higher blood volume, compared to surrounding tissue.

The spectroscopic power of optical imaging, along with the ability to quantify physiological parameters of human breast, have opened up a new opportunity for assessing metabolic and physiological activities of human breast during treatment.

**Table 1.** Optical parameters of tumor and background breast tissue.

| Unknown coefficients | reconstructed values $\lambda = 670$ nm | reconstructed values $\lambda = 785$ nm |
|---|---|---|
| Absorption (background) | 0.0029 $mm^{-1}$ | 0.0024 $mm^{-1}$ |
| Scattering (background) | 1.20 $mm^{-1}$ | 1.10 $mm^{-1}$ |
| Absorption (tumor) | 0.0071 $mm^{-1}$ | 0.0042 $mm^{-1}$ |
| Scattering (tumor) | 1.76 $mm^{-1}$ | 1.6 $mm^{-1}$ |

## 6. Quantitative fluorescence imaging and spectroscopy

As mentioned in Section 2, advances in the molecular biology of disease processes, new immunohistopathological techniques, and the development of specific fluorescently-labeled cell surface markers have led a revolution in research on the molecular origins of disease processes. On the other hand, reliable, sensitive, and specific, non-invasive techniques are needed for in vivo determinations of abnormalities within tissue. If successfully developed, noninvasive 'optical biopsies' may replace invasive, destructive biopsies and provide the advantages of smaller sampling errors, reduction in cost and time for diagnosis resulting in easier integration of diagnosis and therapy by following progression of disease or its regression in response to therapy. Clinically practical fluorescence imaging techniques must meet several requirements. First, the pathology under investigation must not lie at a depth where the attenuation of the signal results in a poor signal-to-noise ratio and resolvability. Second, the specificity of the marker must be high enough that one can clearly distinguish between normal and abnormal lesions. Finally, one must have a robust image reconstruction algorithm which enables one to quantify the fluorophore concentration at a given depth.

The choices of projects in this area of research are dictated by the importance of the problem, and the impact of the solution on health care. Below, the rationale of two projects, that the unit at the National Institutes of Health is pursuing, are described.

Sjøgren's Syndrome (SS) has been chosen as an appropriate test case for developing a noninvasive optical biopsy based on 3D localization of exogenous specific fluorescent labels. SS is an autoimmune disease affecting minor salivary glands which are near (0.5 to 3.0 mm below) the oral mucosal surface [58]. Therefore the target pathology is relatively accessible to noninvasive optical imaging. The hydraulic conductivity of the oral mucosa is relatively high, which along with the relatively superficial location of the minor salivary glands, makes topical application and significant labeling of diseased glands with large fluorescent molecules easy to accomplish. We expect that fluorescent ligands (e.g., fluorescent antibodies specific to $CD4^+$ T cell-activated lymphocytes infiltrating the salivary glands) will bind specifically to the atypical cells in the tissue, providing high contrast and a quantitative relationship to their concentration (and therefore to the stage of the disease process). The major symptoms (dry eyes and dry mouth due to decreased tear and saliva secretion) are the result of progressive immune-mediated dysfunction of the lacrimal and salivary glands. Currently, diagnosis is made by excisional biopsies of the minor salivary glands in the lower lip. This latter exam, though considered the best criterion for diagnosis, involves a surgical procedure under local anesthesia followed by post-operative discomfort (swelling, pain) and frequently a temporary loss of sensation of the lower lip biopsy site. Additionally, biopsy is inherently subject to sampling errors and the preparation of histopathological slides is time consuming, complicated, expensive and requires the skills of several professionals (dentist, pathologist, laboratory technician). Thus, there is a clear need for a noninvasive diagnostic procedure which reflects the underlying gland pathology and has good specificity. A quantitative noninvasive assay would also allow repetition of the test to monitor disease progression and the effect of treatment. However, the quantification of fluorophore concentration within the tissue from surface images requires determining the intensities of different fluorophore sources, as a function of depth

and transverse distance and predicting the 3D distribution of fluorophores within the tissue from a series of images [57,59,60].

The second project involves the lymphatic imaging-sentinel node detection. The stage of cancer at initial diagnosis often defines prognosis and determines treatment options. As part of the staging procedure of melanoma and breast cancer, the primary lymphatic draining site is exposed and multiple lymph nodes are removed and examined histologically for the presence of malignant cells. Because it is not obvious which nodes to remove at the time of resection of the primary tumor, the standard surgical practice for determining the stage of breast cancer involves dissection of as many lymph nodes as feasible. Since such extensive removal of lymphatic tissue frequently results in compromised lymphatic drainage in the examined axilla, alternatives have been sought to define the stage at the time of primary resection. A recent advance in lymph node interrogation has been the localization and removal of the 'sentinel' node. Although there are multiple lymphatic channels available for trafficking from the primary tumor, the assumption was made that the anatomic location of the primary tumor in a given individual drains into lymphatic channels in an orderly and reproducible fashion. If that is in fact the case, then there is a pattern by which lymphatic drainage occurs. Thus, it would be expected that malignant cells from a primary tumor site would course from the nearest and possibly most superficial node into deeper and more distant lymphatic channels to ultimately arrive in the thoracic duct, whereupon malignant cells would gain access to venous circulation. The sentinel node is defined to be the first drainage node in a network of nodes that drain the primary cancer. Considerable evidence has accrued validating the clinical utility of staging breast cancer by locating and removing the sentinel node at the time of resection of the primary tumor. Currently, the primary tumor is injected with a radionucleotide one day prior to removal of the primary tumor. Then, just before surgery, it is injected with visible dye. The surgeon localizes crudely the location of the sentinel node using a hand-held radionucleotide detector, followed by a search for visible concentrations of the injected dye. The method requires expensive equipment and also presents the patient and hospital personnel with the risk of exposure to ionizing radiation. As an alternative to the radionucleotide, we are investigating the use of IR-dependent fluorescent detection methods to determine the location of sentinel node(s).

For in vivo fluorescent imaging, the technological complication factor is the strong attenuation of light as it passes through tissue which deteriorates the signal-to-noise ratio of detected photons. Fortunately, development of fluorescent dyes (such as porphyrin and cyanine) that excite and reemit in the 'biological window' at near-infrared (NIR) wavelengths, where scattering and absorption coefficients are relatively low, have provided new possibilities for deep fluorescence imaging in tissue. The theoretical complication occurs at depths greater than 1 mm where photons in most tissues enter a diffusion-like state with a large dispersion in their path-lengths. Indeed, the fluorescent intensity collected from deep tissue structures depends not only on the location, size, concentration, and intrinsic characteristics (e.g., lifetime, quantum efficiency) of the fluorophores, it depends also on the scattering and absorption coefficients of the tissue at both the excitation and emission wavelengths. Hence, in order to extract intrinsic characteristics of fluorophores within tissue, it is necessary to describe the statistics of photon pathlengths which depend on all these differing parameters.

Obviously, the modeling of fluorescent light propagation depends on the kinds of experiments that one plans to perform. For example, for frequency-domain measurements, Patterson and Pogue [61] used the diffusion approximation of the transport equation to express their results in terms of a product of two Green's function propagators multiplied by a term that describes the probability of emission of a fluorescent photon at the site. One Green's function describes the movement of an incident photon to the fluorophore, and the other describes movement of the emitted photon to the detector. In this representation, the amount of light emitted at the site of the fluorophore is directly proportional to the total amount of light impinging on the fluorophore, with no account for the variability in the number of visits by a photon before an exciting transformation. Since a transformation on an early visit to the site precludes a transformation on all later visits, this results in an overestimation of the number of photons which have a fluorescence transformation at a particular site. This overestimation is important when fluorescent absorption properties are spatially inhomogeneous and largest at later arrival times. RWT has been used to allow for this spatial

inhomogeneity by introducing the multiple-passage probabilities concept, thus rendering the model more physically plausible [62]. Another incentive to devise a general theory of diffuse fluorescence photon migration is the capability to quantify local changes in fluorescence lifetime. By selecting fluorophore probes with known lifetime dependence on specific environmental variables, lifetime imaging enables one to localize and quantify such metabolic parameters as temperature and pH, as well as changes in local molecular concentrations in vivo.

In the probabilistic RWT model, the description of a photon path may be divided into three parts: the path from the photon source to a localized, fluorescing target; the interaction of the photon with the fluorophore; and finally, the path of the fluorescently emitted photon to a detector. Each part of the photon path may be described by a probability: first, the probability that an incident photon will arrive at the fluorophore site; second, the probability that the photon has a reactive encounter with the fluorophore and the corresponding photon transit delay, which is dependent on the lifetime of the fluorophore and the probability of the fluorophore emitting a photon; and third, the probability that the photon emitted by the fluorophore travels from the reaction site to the detector. Each of these three sequences is governed by a stochastic process. The mathematical description of the three processes is extremely complicated. The complete solution for the probability of fluorescence photon arrival at the detector is [63]

$$\hat{\gamma}(r,s,r_0) = \frac{\eta\Phi\hat{p}'_\xi(r \mid s)\hat{p}_\xi(s \mid r_0)}{\langle\Delta n\rangle(1-\eta)[\exp(\xi)-1] + \{\eta\langle\Delta n\rangle[\exp(\xi)-1]+1\}\left\{1+\frac{1}{8}\left(\frac{3}{\pi}\right)^{3/2}\sum_{j=1}^{\infty}\frac{\exp(-2j\xi)}{j^{3/2}}\right\}} \tag{14}$$

where $\eta$ is the probability of fluorescent absorption of an excitation wavelength photon, $\Phi$ is the quantum efficiency of the fluorophore which is the probability that an excited fluorophore will emit a photon at the emission wavelength, $\langle\Delta n\rangle$ is the mean number of steps the photon would have taken had the photon not been exciting the fluorophore (which corresponds to the fluorophore lifetime in random walk parameters), $\xi$ is a transform variable corresponding to the discrete analog of the Laplace transform and may be considered analogous to frequency. The probability of a photon going from the excitation source to the fluorophore site is $\hat{p}_\xi(s \mid r_0)$, and the probability of a fluorescent photon going from the fluorophore site to the detector is $\hat{p}'_\xi(r \mid s)$; the prime indicates that the wavelength of the photon has changed and therefore the optical properties of the tissue may be different. In practice, this solution is difficult to work with, so some

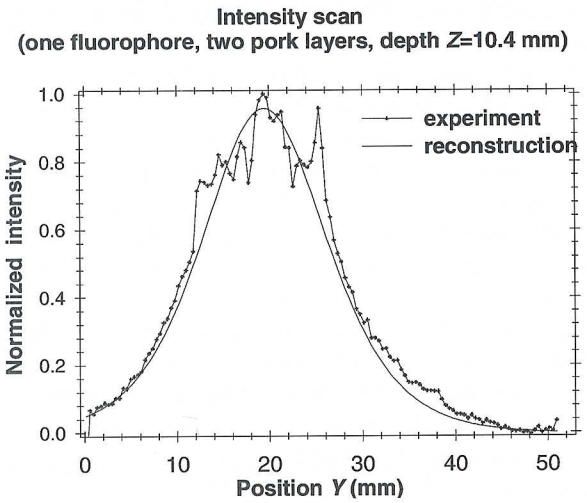


**Figure 6.** Intensity scan of a fluorophore 10.4 mm below the tissue surface.

simplifying assumptions are desired. With some simplification the result in the frequency domain is:

$$\hat{\gamma}(r, s, r_0) = \eta \Phi \left\{ \hat{p}'_\xi(r \mid s) \hat{p}_\xi(s \mid r_0) - \xi(\Delta n) \hat{p}'_\xi(r \mid s) \hat{p}_\xi(s \mid r_0) \right\}. \quad (15)$$

The inverse Laplace transform of this equation gives the diffuse fluorescent intensity in the time-domain, and the integral of the latter over time leads to CW measurements. The accuracy of such cumbersome equations is tested in well-defined phantoms and fluorophores embedded in ex-vivo tissue. In *figure 6*, a line scan of fluorescent intensity collected from 500 $\mu m^3$ fluorescent dye (Molecular Probe, far red microspheres: 690 nm excitation; 720 nm emission), embedded in 10.4 mm porcine tissue with a lot of heterogeneity (e.g., fat), are presented. The solid line is the corresponding RWT fit. Our inverse algorithm written in C++ was able to construct the depth of the fluorophore with 10% accuracy. Knowing the heterogeneity of the tissue (seen in the intensity profile) this method presents huge potential to interrogate tissue structures deeply embedded in tissue for which specific fluorescent labeling such as antibodies for cell surfaces exists.

## 7. Conclusion

A clinically useful optical imaging device requires multi-disciplinary and multi-step approaches. At the desk, one devises quantitative theories, and develop methodologies applicable to in vivo quantitative tissue spectroscopy and tomographic imaging in different imaging geometries (i.e., transmission or reflection), different types of measurements (e.g., steady-state or time-resolved). Effects of different optical sources of contrast such as endogenous or exogenous fluorescent labels, variations in absorption (e.g., hemoglobin or chromophore concentration) and scattering should be incorporated in the model. At the bench, one designs and conducts experiments on tissue-like phantoms and runs computer simulations to validate the theoretical findings. If successful, one tries to bring the imaging or spectroscopic device to the bedside. For this task, one must foster strong collaborations with physicians who can help to identify physiological sites where optical techniques may be clinically practical and can offer new diagnostic knowledge and/or less morbidity over existing methods. An important intermediate step is the use of animal models for pre-clinical studies. Overall, this is a complicated path. However, the spectroscopic power of light, along with the revolution in molecular characterization of disease processes has created a huge potential for in-vivo optical imaging and spectroscopy. Maybe the twenty-first century will be the second 'siecle des lumieres'.

**Acknowledgement.** I warmly thank my colleagues, Dr. Victor Chernomordik, Dr. David Hattery, Behdad Besharatian, Kristin Gerdelman, and Nina Paolella, for their help while preparing this article. Special thanks also go to Drs Herbert Rinneberg (Physikalich.-Techniche-Bundesanstalt, Berlin) and Brian Pogue (Dartmouth College) for providing us with optical images.

## References

[1] Born M., Wolf E., Principles in Optics, 7th edition, Cambridge University Press, Cambridge, UK, 1999.
[2] Young A.T., Rayleigh Scattering, Phys. Today (1982) 42–48.
[3] Saidi I.S., Jacques S.L., Tittel F.K., Mie and Rayleigh modeling of visible-light scattering in neonatal skin, Appl. Opt. 34 (1995) 7410–7418.
[4] Van Gemert M.J.C., Jacques S.L., Sterenborg H.J.C.M., Star W.M., Skin Optics, IEEE Trans. Biomed. Engng. 36 (12) (1989) 1146–1153.
[5] Marchesini R., Bertoni A., Andreola S., Melloni E., Sicherollo A.E., Extinction and absorption coefficients and scattering phase functions of human tissues in vitro, Appl. Opt. 28 (1989) 2318–2324.
[6] Fishkin J.B., Coquoz O., Anderson E.R., Brenner M., Tromberg B.J., Frequency-domain photon migration measurements of normal and malignant tissue optical properties in a human subject, Appl. Opt. 36 (1997) 10–20.
[7] Troy T.L., Page D.L., Sevick-Muraca E.M., Optical properties of normal and diseased breast tissues: prognosis for optical mammography, J. Biomed. Opt. 1 (1996) 342–355.

[8] Gandjbakhche A.H., Bonner R.F., Nossal R., Scaling relationships for anisotropic random walks, J. Stat. Phys. 69 (1992) 35–53.
[9] Wagnieres G.A., Star W.M., Wilson B.C., In vivo fluorescence spectroscopy and imaging for oncological applications, Photochem. Photobiol. 68 (1998) 603–632.
[10] Weissleder R., A clearer vision for in vivo imaging, Nature Biotechnol. 19 (2001) 316–317.
[11] Kamalov V.F., Struganova I.A., Yoshihara K., Temperature dependent radiative lifetime of J-aggregates, J. Phys. Chem. 100 (1996) 8640–8644.
[12] Mordon S., Devoisselle J.M., Maunoury V., In vivo pH measurement and imaging of a pH-sensitive fluorescent probe (5–6 carboxyfluorescein): instrumental and experimental studies, Photochem. Photobiol. 60 (1994) 274–279.
[13] Hutchinson C.L., Lakowicz J.R., Sevick-Muraca E.M., Fluorescence lifetime-based sensing in tissues: a computational study, Biophys. J. 68 (1995) 1574–1582.
[14] Jobsis F.F., Noninvasive infrared monitoring of cerebral and myocardial oxygen sufficiency and circulatory parameters, Science 198 (1977) 1264–1267.
[15] Farrell T.J., Patterson M.S., Wilson B., A diffusion theory model of spatially resolved, steady-state diffuse reflectance for the noninvasive determination of tissue optical properties in vivo, Med. Phys. 9 (1992) 879–888.
[16] Jarry G., Ghesquiere S., Maarek J.M., Fraysse F., Debray S., Bui M.-H., Laurent D., Imaging mammalian tissues and organs using laser collimated transillumination, J. Biomed. Engng. 6 (1984) 70–74.
[17] Jackson P.C., Stevens P.H., Smith J.H., Kear D., Key H., Wells P.N.T., Imaging mammalian tissues and organs using laser collimated transillumination, J. Biomed. Engng. 6 (1987) 70–74.
[18] Kaneko M. et al., Construction of a laser transmission photo-scanner: pre-clinical investigation, Radiat. Med. 7 (1989) 129–134.
[19] Wang L., Ho P.P., Zhang G., Alfano R.R., Time-resolved Fourier spectrum and imaging in highly scattering media, Appl. Opt. 32 (1993) 5043–5048.
[20] Schmitt J.M., Gandjbakhche A.H., Bonner R.F., Use of polarized light to discriminate short-path photons in a multiply scattering medium, Appl. Opt. 31 (1992) 6535–6546.
[21] Inaba H., Coherent detection imaging for medical laser tomography, in: Muller G. (Ed.), Medical Optical Tomography: Functional Imaging and Monitoring, SPIE, Bellingham, WA, 1993, pp. 317–347.
[22] Inaba H., Toida M., Ichmua T., Optical computer-assisted tomography realized by coherent detection imaging incorporating laser heterodyne method for biomedical applications, in: SPIE Proc., Vol. 1399, 1990, pp. 108–115.
[23] Schmidt A., Corey R., Saulnier P., Imaging through random media by use of low-coherence optical heterodyning, Opt. Lett. 20 (1995) 404–406.
[24] Colak S.B., Papaioannou D.G., T'Hooft G.W., van der Mark M.B., Schomberg H., Paasschens J.C.J., Melissen J.B.M., van Austen N.A.A.J., Tomographic image reconstruction from optical projections in light diffusing media, Appl. Opt. 36 (1997) 180–213.
[25] Wang L., Ho P.P., Liu C., Zhang G., Alfano R.R., Ballistic 2D imaging through scattering walls using an ultrafast optical Kerr gate, Science 253 (1991) 769–771.
[26] Hebden J.C., Hall D.J., Firbank M., Delpy D.T., Time-resolved optical imaging of a solid tissue-equivalent phantom, Appl. Opt. 34 (1995) 8038–8047.
[27] Hebden J.C., Evaluating the spatial resolution performance of a time-resolved optical imaging system, Med. Phys. 19 (1992) 1081–1087.
[28] Cubeddu R., Pifferi A., Taroni P., Torriceli A., Valentini G., Time-resolved imaging on a realistic tissue phantom: $\mu_s'$ and $\mu_a$ images versus time-integrated images, Appl. Opt. 35 (1996) 4533–4540.
[29] Grosenick D., Wabnitz H., Rinneberg H., Moesta K.Th., Schlag P., Development of a time-domain optical mammograph and first in-vivo application, Appl. Opt. 38 (1999) 2927–2943.
[30] Bashkansky M., Adler C., Reintjes J., Coherently amplified Raman polarization gate for imaging through scattering media, Opt. Lett. 19 (1994) 350–352.
[31] Yoo K.M., Xing Q., Alfano R.R., Imaging objects hidden in highly scattering media using femtosecond second-harmonic-generation cross-correlation time gating, Opt. Lett. 16 (1991) 1019–1021.
[32] Faris G.W., Banks M., Upconverting time gate for imaging through highly scattering media, Opt. Lett. 19 (1994) 1813–1815.
[33] Hebden J.C., Arridge S.R., Delpy D.T., Optical imaging in medicine I: experimental techniques, Phys. Med. Biol. 42 (1997) 825–840.
[34] Lakowitz J.R., Brendt K., Frequency domain measurements of photon migration in tissues, Chem. Phys. Lett. 166 (1990) 246–252.
[35] Franceschini M.A., Moesta K.T., Fantini S., Gaida G., Gratton E., Jess H., Mantulin W.W., Seeber M., Schlag P.M., Kaschke M., Frequency-domain techniques enhance optical mammography: initial clinical results, Proc. Nat. Acad. Sci., Med. Sci. 94 (1997) 6468–6473.

[36] Fishkin J.B., Coquoz O., Anderson E.R., Brenner M., Tromberg B.J., Frequency-domain photon migration measurements of normal and malignant tissue optical properties in a human subject, Appl. Opt. 36 (1997) 10–20.
[37] Tromberg B.J., Coquoz O., Fishkin J., Pham T., Anderson E.R., Butler J., Cahn M., Gross J.D., Venugopalan V., Pham D., Non-invasive measurements of breast tissue optical properties using frequency-domain photon migration, Philos. Trans. R. Soc. London Ser. B 352 (1997) 661–668.
[38] Duderstadt J.J., Hamilton L.J., Nuclear Reactor Analysis, Wiley, New York, 1976.
[39] Case K.M., Zweifel P.F., Linear Transport Theory, Addison-Wesley, Reading, MA, 1967.
[40] Ishimaru A., Wave Propagation and Scattering in Random Media, Academic Press, New York, 1978.
[41] Patterson M.S., Chance B., Wilson B., Time resolved reflectance and transmittance for the non-invasive measurement of tissue optical properties, Appl. Opt. 28 (1989) 2331–2336.
[42] Arridge S.R., Hebden J.C., Optical imaging in medicine: II. Modelling and reconstruction, Phys. Med. Biol. 42 (1997) 841–853.
[43] Nioka S., Miwa M., Orel S., Schnall M., Haida M., Zhao S., Chance B., Optical imaging of human breast cancer, Adv. Exp. Med. Biol. 361 (1994) 171–179.
[44] Fantini S., Walker S.A., Franceschini M.A., Kaschke M., Schlag P.M., Moesta K.T., Assessment of the size, position, and optical properties of breast tumors in vivo by noninvasive optical methods, Appl. Opt. 37 (1998) 1982–1989.
[45] Maris M., Gratton E., Maier J., Mantulin W., Chance B., Functional near-infrared imaging of deoxygenated haemoglobin during exercise of the finger extensor muscles using the frequency-domain techniques, Bioimaging 2 (1994) 174–183.
[46] Pogue B.W., Paulsen K.D., High-resolution near-ingrared tomographic imaging simulations of the rat cranium by use of a priori magnetic resonance imaging structural imformation, Opt. Lett. 23 (1998) 1716–1718.
[47] Bonner R.F., Nossal R., Havlin S., Weiss G.H., Model for photon migration in turbid biological media, J. Opt. Soc. Am. A 4 (1987) 423–432.
[48] Gandjbakhche A.H., Weiss G.H., Random walk and diffusion-like models of photon migration in turbid media, in: Wolf E. (Ed.), Progress in Optics, XXXIV, Elsevier, 1995, pp. 333–402.
[49] Gandjbakhche A.H., Nossal R., Bonner R.F., Scaling relationships for theories of anisotropic random walks applied to tissue optics, Appl. Opt. 32 (4) (1993) 504–516.
[50] Chernomordik V., Nossal R., Gandjbakhche A.H., Point spread functions of photons in time-resolved transillumination experiments using simple scaling arguments, Med. Phys. 23 (1996) 1857–1861.
[51] Gandjbakhche A.H., Weiss G.H., Bonner R.F., Nossal R., Photon path-length distributions for transmission through optically turbid slabs, Phys. Rev. E 48 (2) (1993) 810–818.
[52] Hawrysz D.J., Sevick-Muraca E.M., Developments toward diagnostic breast cancer imaging using near-infrared optical measurements and fluorescent contrast agents, Neoplasia 2 (2000) 388–417.
[53] Cutler M., Transillumination as an aid in the diagnosis of breast lesions, Surg. Gynecol. Obstet. 48 (1929) 721–728.
[54] Gandjbakhche A.H., Nossal R., Bonner R.F., Resolution limits for optical transillumination of abnormalities deeply embedded in tissues, Med. Phys. 21 (2) (1994) 185–191.
[55] Gandjbakhche A.H., Chernomordik V., Hebden J.C., Nossal R., Time-dependent contrast functions for quantitative imaging in time-resolved transillumination experiments, Appl. Opt. 37 (1998) 1973–1981.
[56] Chernomordik V., Hattery D., Pifferi A., Taroni P., Torricelli A., Valentini G., Cubeddu R., Gandjbakhche A.H., A random walk methodology for quantification of the optical characteristics of abnormalities embedded within tissue-like phantoms, Opt. Lett. 25 (2000) 951–953.
[57] Gandjbakhche A.H., Gannot I., Quantitative fluorescence imaging of specific markers of diseased tissue, IEEE J. Sel. Topics Quant. Electron 2 (1996) 914–921.
[58] Fox R.I. (Ed.), Sjogren Syndrome, Rheumatic Disease Clinic of North America, 1992.
[59] Gannot I., Bonner R.F., Gannot G., Fox P.C., Smith P., Gandjbakhche A.H., Optical simulations of a non-invasive technique for the diagnosis of diseased salivary glands in-situ, Med. Phys. 25 (1998) 1139–1144.
[60] Chernomordik V., Hattery D., Gannot I., Gandjbakhche A.H., Inverse method 3D reconstruction of localized in-vivo fluorescence. Application to Sjøgren Syndrome, IEEE J. Sel. Topics Quant. Electron 5 (1999) 930–935.
[61] Patterson M.S., Pogue B.W., Mathematical model for time-resolved and frequency-domain fluorescence spectroscopy in biological tissue, Appl. Opt. 33 (1994) 1963–1974.
[62] Gandjbakhche A.H., Bonner R.F., Nossal R., Weiss G.H., Effects of multiple passage probabilities on fluorescent signals from biological media, Appl. Opt. 36 (1997) 4613–4619.
[63] Hattery D., Chernomordik V., Loew M., Gannot I., Gandjbakhche A., Analytical solutions for time-resolved fluorescence lifetime imaging in a turbid medium such as tissue, J. Opt. Soc. Am. A 18 (2001) 1523–1530.